Laser-induced damage threshold of camera sensors and micro-optoelectromechanical systems

Bastian Schwarz
Gunnar Ritt
Michael Koerber
Bernd Eberle

Laser-induced damage threshold of camera sensors and micro-optoelectromechanical systems

Bastian Schwarz,* Gunnar Ritt, Michael Koerber, and Bernd Eberle
Fraunhofer Institute of Optronics, System Technologies, and Image Exploitation, Ettlingen, Germany

Abstract. The continuous development of laser systems toward more compact and efficient devices constitutes an increasing threat to electro-optical imaging sensors, such as complementary metal–oxide–semiconductors (CMOS) and charge-coupled devices. These types of electronic sensors are used in day-to-day life but also in military or civil security applications. In camera systems dedicated to specific tasks, micro-optoelectromechanical systems, such as a digital micromirror device (DMD), are part of the optical setup. In such systems, the DMD can be located at an intermediate focal plane of the optics and it is also susceptible to laser damage. The goal of our work is to enhance the knowledge of damaging effects on such devices exposed to laser light. The experimental setup for the investigation of laser-induced damage is described in detail. As laser sources, both pulsed lasers and continuous-wave (CW)-lasers are used. The laser-induced damage threshold is determined by the single-shot method by increasing the pulse energy from pulse to pulse or in the case of CW-lasers, by increasing the laser power. Furthermore, we investigate the morphology of laser-induced damage patterns and the dependence of the number of destructive device elements on the laser pulse energy or laser power. In addition to the destruction of single pixels, we observe aftereffects, such as persistent dead columns or rows of pixels in the sensor image. © The Authors. Published by SPIE under a Creative Commons Attribution 3.0 Unported License. Distribution or reproduction of this work in whole or in part requires full attribution of the original publication, including its DOI. [DOI: 10.1117/1.OE.56.3.034108]

1 Introduction

Since the invention of the laser in 1960, laser systems have become more and more powerful and even more compact from year to year. Laser radiation is increasingly becoming a hazard to the human eye as well as to electro-optical imaging sensors—not only in form of laser damage but also due to laser dazzle. Knowing that detectors, such as complementary metal–oxide–semiconductors (CMOS) or charge-coupled devices (CCD), are very sensitive to laser light, there is a strong continued interest in protection measures against dazzling and damaging. At our institute, a lot of effort was put into the investigation of laser protection measures that provide wavelength-independent protection.[1,2] One of our concepts to suppress laser dazzle in camera systems is based on installing a digital micromirror device (DMD) into a focal plane of an optical setup in combination with wavelength multiplexing.[3–5] A scheme of this optical setup and a photograph of the hardened sensor according to this concept are shown in Fig. 1. Without going into the details of this optical setup, one can see that two devices are placed at focal planes: (a) the DMD at the intermediate focal plane and (b) the imaging sensor in the focal plane of the camera lens. Now the question arises as to what would happen if this sensor is exposed to laser irradiation with intensities far beyond the threshold for laser dazzle. Which device will be damaged first? The DMD or the imaging sensor?

From an economic point of view, one would prefer that the imaging sensor is damaged first, because the imaging sensor is quite cheap compared to the DMD. The user of such a system would prefer the DMD to be damaged first. In this case, the DMD acts as a sacrificial element for the imaging sensor. The system could still be used, only some distortions would occur (such as a color distortion or contrast loss) in the sensor image.[6] The magnitude of the distortion would depend on the size of the damage on the DMD.

Of course, there are some publications regarding laser damage thresholds of camera sensors and DMDs. For example, Becker et al.[7,8] studied laser-induced damage of CCD sensors by nanosecond laser pulses at 1064 nm. First functional changes were observed at a fluence value of $0.55~\mathrm{J/cm^2}$. Guo et al.[9] investigated the damage effect on CMOS detectors irradiated by laser pulses at 1064 nm. In the case of nanosecond laser pulses, the damage threshold was around $0.38~\mathrm{J/cm^2}$ and in the case of picosecond laser pulses, they received a threshold value of $0.02~\mathrm{J/cm^2}$.

For the DMD, the maximum power density for homogeneous illumination is specified as $25~\mathrm{W/cm^2}$ in the visible spectral range.[10,11] However, in a publication of Faustov et al.,[12] a damage threshold above 22 mW for a laser wavelength of 633 nm is reported for the case in which the laser light is focused onto a single micromirror ($13.7 \times 13.7~\mu\mathrm{m^2}$). This value corresponds to an irradiance of ~12 $\mathrm{kW/cm^2}$ and is far above the value stated by Texas Instruments. This discrepancy motivated us to perform laser damage experiments with a DMD as well as standard CCD and CMOS cameras.

In this work, we examine the laser damage threshold and the morphology of laser damage in the camera images of

*Address all correspondence to: Bastian Schwarz, E-mail: bastian.schwarz@iosb.fraunhofer.de
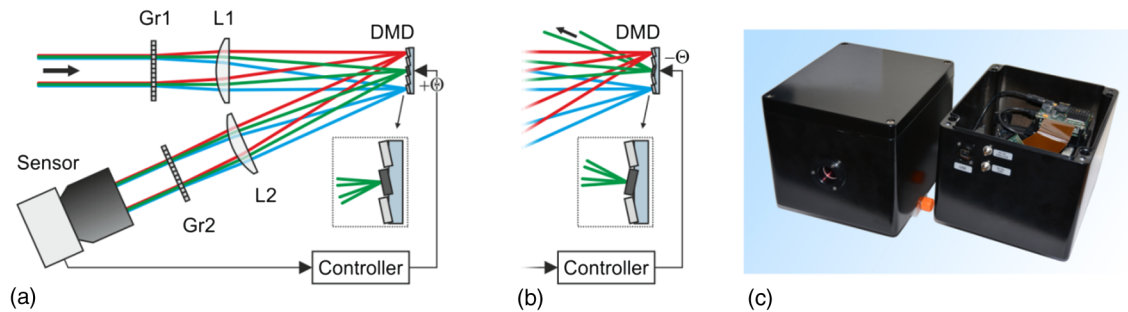
Fig. 1 Concept for hardening a sensor against laser dazzling using a DMD: (a) operation mode for regular imaging, (b) operation mode with high attenuation of dazzling laser light, and (c) photograph of the hardened sensor.

CMOS and CCD devices. The surface of the DMD is investigated by means of the image of a CMOS device. We will return to that later. The results enable us to get first indications, determine which of these devices suffer damage first from laser radiation, and to check if the DMD acts as a sacrificial element in the optical setup.

Detailed knowledge about laser damage thresholds of imaging sensors is not only important for scientists working in the area of laser protection. It is also of interest, for example, to the manufacturers of devices for laser beam characterization. Camera-based laser beam profilers or M^2 measurement systems employ imaging sensors that are directly exposed to a laser beam. They can suffer damage when the laser intensity exceeds the damage threshold.

When using different laser configurations, we expect different damage mechanisms to affect the devices.[13] In the case of irradiation with millisecond- and longer-laser pulses, thermal effects that convert the laser energy into thermal energy are the main damage mechanism. This is related to the melting or vaporization of the material. On the contrary, irradiation with shorter laser pulses calls other damage mechanisms into play. That applies especially for highly transmitting materials, where the damage threshold is rather high. Laser pulses on the order of nanoseconds or picoseconds

cause electrically induced damage due to the corresponding high laser electric field intensity and the short duration of the laser pulse effects, such as dielectric breakdown. During such a breakdown mechanism, the insulator becomes electrically conductive plasma which causes thermal damage in a next step as well as shock damage and mechanical damage. For further details please refer to Ref. 14. We expect, that the disturbance in the output images of the cameras is different for the continuous-wave (CW)-laser and the pulsed laser.

2 Setup and Procedures of the Experiment

2.1 *Instrumental Setup*

The schematic of the experiment is shown in Fig. 2. The sensors under test were irradiated by two different types of laser systems to perform the laser-induced damage tests:

- Pulsed laser system: Nd:YAG laser, operating at a wavelength of 1064 nm with a maximum pulse energy of 300 mJ at a repetition rate of 10 Hz and a spatial Gaussian energy distribution (InnoLas Spitlight Hybrid). We used the second harmonic at a wavelength of 532 nm, generated by a harmonic Generating Assemblies

(a)

(b)
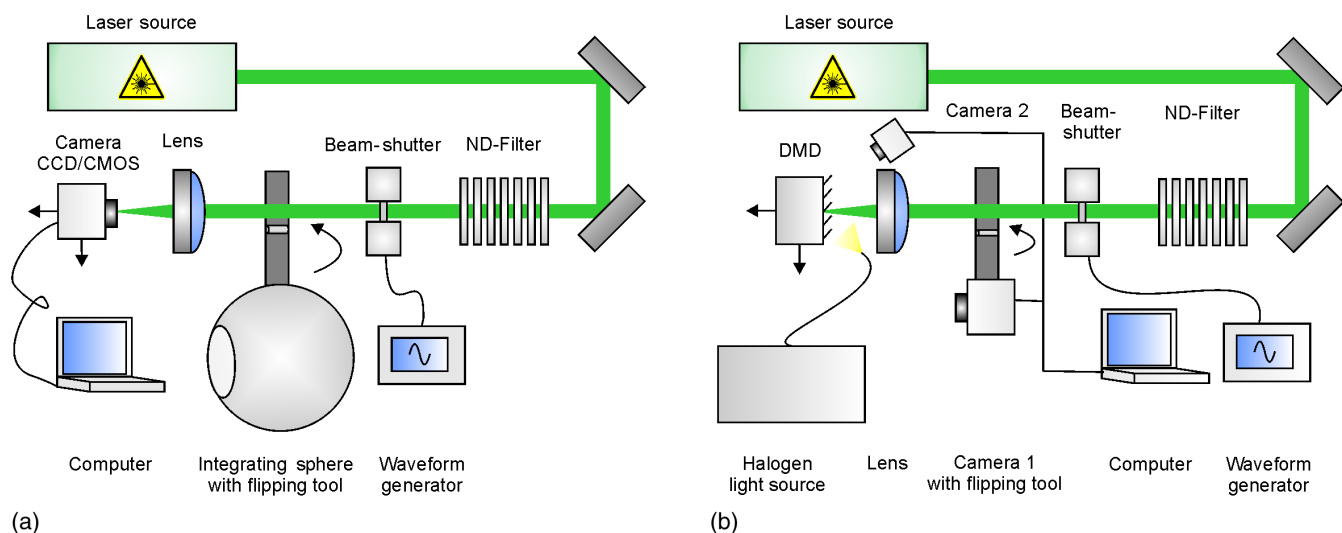
Fig. 2 Experimental setup: (a) configuration for CCD/CMOS damaging testing and (b) configuration for the DMD testing.

containing kaliumtitanylphosphate crystals. The temporal pulse length was 10 ns and the beam diameter was 6 mm ($1/e^2$).

- CW-laser system: Diode-pumped solid-state laser (DPSS, Laser Quantum Ventus 532) with a wavelength of 532 nm and a beam size of 1.5 mm ($1/e^2$). The available laser power exceeded 500 mW.

The incident laser energy of the pulsed laser was adjusted by varying the time delay between the beginning of the flash lamp pulse and the trigger of the Pockels cell. The power level of the CW-laser source was controlled by changing the current of the diode driver from 49% up to 100%.

Furthermore, we used a set of neutral density filters with different optical densities (ODs) ranging from OD 0.5 to OD 3.0. To control different exposure times of the CW-laser source, we used a laser shutter (Uniblitz Shutter Systems VS25). Finally, the laser beam was focused by a lens (Apo-Rodagon N 4.0/80, Qioptiq) with a focal length of $f = 80$ mm and an aperture of $f/5.6$, thus the beam diameter in the focal plane was measured by the beam profiler BP209 from Thorlabs using a scanning slit method. The measurement with the beam profiler took place before the actual experiment. Therefore, we were able to determine the diameter ($1/e^2$) of the laser spot in the focal plane and got a value of $2\omega_1 = 25.7$ μm for the CW-laser source and $2\omega_2 = 28.2$ μm for the pulsed laser source. The effective diameter d_{eff} of a uniform cylindrical beam with the same peak intensity and total power as a cylindrical Gaussian beam is[15]

$$d_{\mathrm{eff}} = \sqrt{2}\omega, \tag{1}$$

and the associated effective spot size A_{eff}

$$A_{\mathrm{eff}} = \frac{\pi\omega^2}{2}. \tag{2}$$

According to this, the effective spot size in the focal plane is $A_{\mathrm{eff}} = 3.12 \times 10^{-6}$ cm^2 for the pulsed laser and $A_{\mathrm{eff}} = 2.59 \times 10^{-6}$ cm^2 for the CW-laser.

The device under test was installed on a 3-D translation stage, so that we could shift the sensor into the focal plane of the lens and each pulse could be exposed to an unused test site (Fig. 2). To detect any changes in the image of the camera, we observed the output signal of the camera on the computer. The experimental setup for the investigation concerning the DMD differed from those concerning the CMOS/CCD sensors. The DMD was also put in the focal plane, but in contrast to the experiments concerning the CMOS/CCD cameras, we used an observer camera [camera 2 in Fig. 2(b), VRmagic VRmFC-22/BW] outside the optical axis to record the position of the laser spot on the DMD and a second observing camera [camera 1 in Fig. 2(b), The Imaging Source DFK22AUC03], which could be flipped into the optical axis, so we could take a picture of the DMD before and after each laser shot to detect whether damage occurred or not.

To compare the output images of the cameras before and after each shot, we illuminated the cameras as uniformly as possible. For that purpose, we used an integrating sphere (connected to a stabilized fiber-coupled light source SLS201/M from Thorlabs), which could be flipped into the beam path in front of the lens. In the case of the DMD sensor, we illuminated the sensor from outside the optical axis with a halogen cold light source (Schott KL 255 LCD) so that the center of the DMD is illuminated as uniformly as possible. Note that the micromirrors' normal and the optical axes form an angle of $+12$ deg to the beam axis in the "on" position and an angle of -12 deg in the "off" position with the result that in one position the light was reflected to observing camera 1 and in one it was not.

The experiment described was performed using monochromatic and color CMOS cameras including an imaging sensor Aptina MT9V024 with a resolution (horizontal × vertical) of 744×488 pixels and a pixel size of 6 μm × 6 μm. We also examined the damage formation of monochromatic and color CCD cameras operating with an imaging sensor (monochromatic: Sony ICX098BQ, color: Sony ICX098BL) at a resolution of 640×480 pixels and

**Table 1** Specifications of the samples under test.

Test sample	The Imaging Source DFK21AU04 (color)	The Imaging Source DMK21AU04 (monochromatic)	The Imaging Source DFK22AUC03 (color)	The Imaging Source DMK22AUC03 (monochromatic)	Texas Instruments DLP Discovery 4100 Development Kit
Device	Sony ICX098BQ	Sony ICX098BL	Aptina MT9V024	Aptina MT9V024	Texas Instruments DLP7000
Device type	CCD	CCD	CMOS	CMOS	DMD
Format (in.)	1/4	1/4	1/3	1/3	0.7
Resolution (H × V) (px)	640 × 480	640 × 480	744 × 480	744 × 480	1024 × 768
Pixel size (H × V) (μm^2)	5.6 × 5.6	5.6 × 5.6	6 × 6	6 × 6	13.68 × 13.68
Bit depth (bit)	8	8	8	8	—
Sensitivity (lx)	0.1	0.03	5	0.1	—
IR cut filter	Yes	No	Yes	No	—
Shutter	Global	Global	Global	Global	—
Exposure time used in the experiment (ms)	120	120	188	188	—

a pixel size of 5.8 μm $\times$ 5.8 μm. The third device under test was a DMD with 1024×768 micromirrors (Texas Instruments DLP7000). All the investigated samples were encapsulated with a protecting glass plate, so we did not expect any contamination (e.g., dust particles) directly on the bare imaging sensor. It can, therefore, be considered that there is no influence on the measured damage thresholds by contamination. Of course, impurities in the starting materials used in sensor production cannot be excluded. The distance from the surface of the cover glass to the surface of the imaging sensor was about 1.94 ± 0.15 mm in case of the CMOS and CCD cameras and the distance from the surface of the cover glass to the surface of the mirror array

was about 2.9 ± 0.1 mm in case of the DMD. The distance corresponded approximately to the double of the Rayleigh range. This means that the laser power density or the laser pulse energy density on the glass surface was significantly lower than the one on the surface of the imaging sensor. All samples are listed in Table 1.
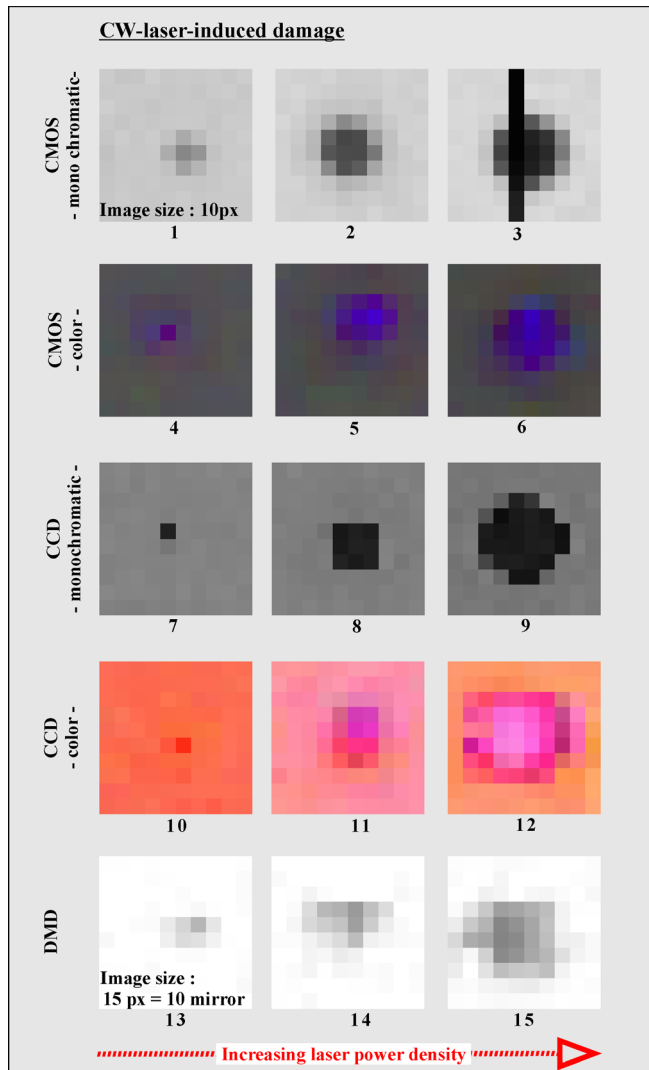
2.2 Implementation of the Experiment

The experiments did not take place in a classified clean room. Therefore, we had to ensure that the protecting glass plates of the imaging sensors were clean from harmful dust and dirt before each test procedure. The test site of
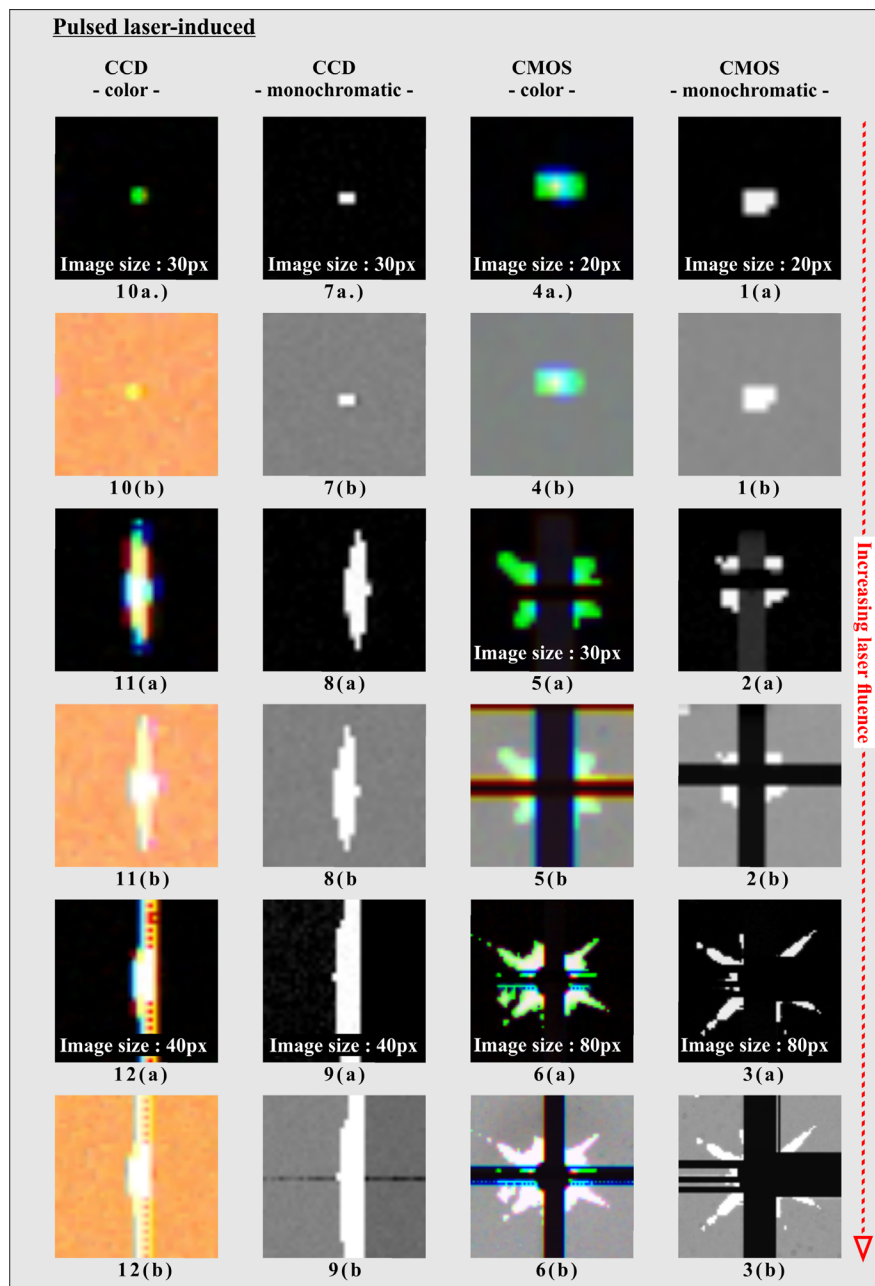
Fig. 3 Raw images of various monochrome and color cameras showing pulsed laser-induced damages in the (a) dark images and (b) in the bright images. The laser fluence used to cause damage increases from top to bottom.

the investigated object was positioned in the focal plane. To measure the damage threshold, we used the 1-on-1 test mode, so each test site was irradiated by one pulse or in the case of CW-laser radiation for a certain exposure time (0.25, 1, 5, and 10 s). Before each laser shot, we took two reference images: an illuminated image (flat-field) and a dark-frame with the same exposure time as we used taking the raw image. In the following, we exposed the sensor with a highly attenuated laser beam, so that no damage could occur to the sensor. We captured a picture during this laser irradiation with the effect that we could determine the positon of the impact of the laser beam on the sensor. After the irradiation with high-power/pulse energy, we took an unexposed image (dark image) and an illuminated image (bright image). Finally, we changed the test site equally whether the sample was damaged or not and repeated the whole procedure after increasing the laser power/pulse energy. Figures 3 and 4 show a selection of raw images of the inflicted damage with and without illumination.

3 Data Analysis and Results

3.1 *Image Processing*

In the case of pulsed laser irradiation, the damaged area in dark images and bright images appeared in the same shape. For the sake of simplicity, we used the dark images to evaluate the damage threshold. We cut the corresponding area first and then subtracted each image with a reference dark-frame (see Fig. 5). In the case of CW-laser irradiation, we used the bright images for evaluation, because there was no damage visible in the dark images. We corrected each raw image by flat-field correction. This was done by removing the DC offset signal by subtracting the dark-frame from the raw image and multiplying it with the normalized flat-field correction image.[16] Color images were converted into grayscale. Finally, we defined damage as a 10% deviation from intensity of the normalized and scaled reference image. Based on this threshold, we converted the postcorrection image into a binary image, so that all pixel values below the threshold
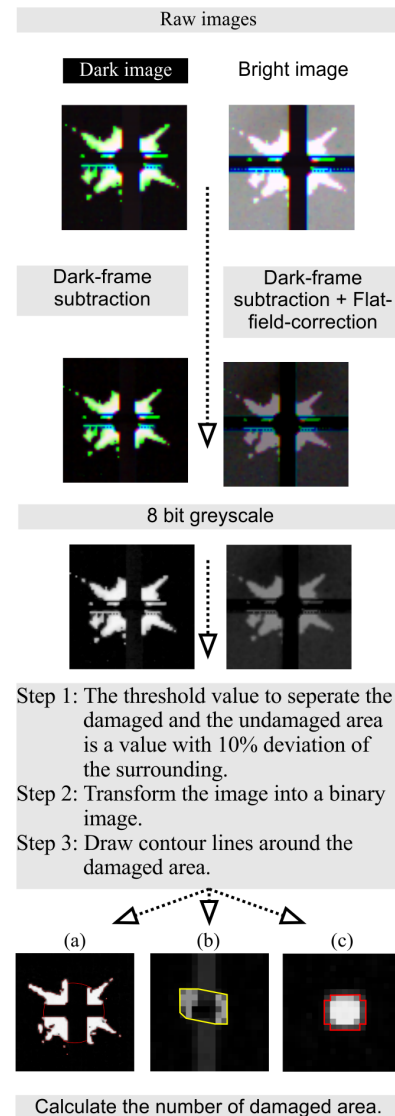

Fig. 4 Raw images of various monochrome and color cameras and the DMD showing pulsed laser-induced damages in the bright images. The laser power density used to cause damage increases from left to right.

Fig. 5 Steps of image processing in case of an illuminated camera image (bright image) and an unexposed camera image (dark image).

value are set to 0 and those above this value to 1. Afterward, we drew a contour line around all pixels with value 1 and, finally, we calculated the area inside this contour.

As long as the laser damage resembles a circular disc, this method is quite easy to apply, see Fig. 5(c). However, for larger laser powers/pulse energies, some deviations can occur:

- Line damage: This means that complete columns or rows of pixels corresponding to the position of the laser spot have failed. Line damage can occur in two ways: only columns or rows fail, see Fig. 5(b), or columns and rows fail, see Fig. 5(a).
- The damage pattern can be star shaped [see Fig. 5(a)].

In the case of single line damage, the contour line is a convex hull around all pixels with the value 1 [see yellow line in Fig. 5(b)]. In the case of star-shaped damage, including line damage, the damaged area was also marked by contour lines. Additionally, the mean distance from the position of the laser spot center on the surface to each outer edge right beside the line damage was determined. After that, a mean circle was computed into the image [see thin red line in Fig. 5(a)]. We defined the damaged area as all pixels that were contained either within the contour or within this mean circle.

3.2 Estimation of the Damage Threshold Based on Thermal-Induced Damages

A logarithmic relationship between the damaged area and laser pulse energy is used to determine the damage threshold and is described in various other experiments.[17–20] In their work, the authors observed by microscope images the evolution of a series of concentric rings, generated through the exposure of ultrashort laser pulses, which they called a specific amorphous ring pattern. Apparently, the ring formation is associated with photo-thermal damage of the subject due to laser radiation. The spatial intensity distribution of a Gaussian laser beam is described as

$$\Phi(r) = \Phi_0 e^{-2\frac{r^2}{\omega_0^2}}. \tag{3}$$

Knowing that the intensity at the rim of the damaged area i with distance r_i from the center of the laser spot corresponds to the damage threshold Φ_{th}, we get

$$r_i^2 = \frac{\omega_0^2}{2\pi} \ln\left[\frac{\Phi}{\Phi_{th}}\right]. \tag{4}$$

In the case of pulsed lasers, the laser-induced damage threshold (LIDT) of absorbing materials is a constant value if measured in terms of J/cm^{-2} so Φ corresponds to the applied laser fluence F, and in the case of CW-laser radiation, the LIDT is a constant value if measured in W/cm^{-2} so Φ corresponds to the irradiance. The distance r_i is the outer radius of the damaged area.[21] The relationship of Eq. (4) also applies in the case of the ablation caused by nanosecond pulses.[22] Following this idea, we plotted the area of the damaged surface of the detector material in pixels versus the fluence or the power density in a semilog plot, respectively, and fitted straight lines to the data according to Eq. (4). The only difference from other experiments is

Table 2 Groups of laser-induced impact on the devices

Group	Description
I	No damage is observed
II	Spot damage occurs (CMOS and CCD camera)
III	Spot damage and line damage occurs (CMOS camera), spot damage elongates in vertical direction and finally transfers into full line damage (CCD camera)
IV	Star-shaped spot damage including full line damage (CMOS camera)

that we did not look at the physically damaged area of the detector material. Moreover, we were interested in the laser-induced damage, which became visible in the output camera image. We defined the "reconstructed beam diameter" (RBD) as the beam diameter we got from the slope of Eq. (4). It represents the required beam diameter of the laser source on the surface of the test object, if the expansion of disturbance in the camera image resembled the physical damage in the sensor.

(a)

(b)
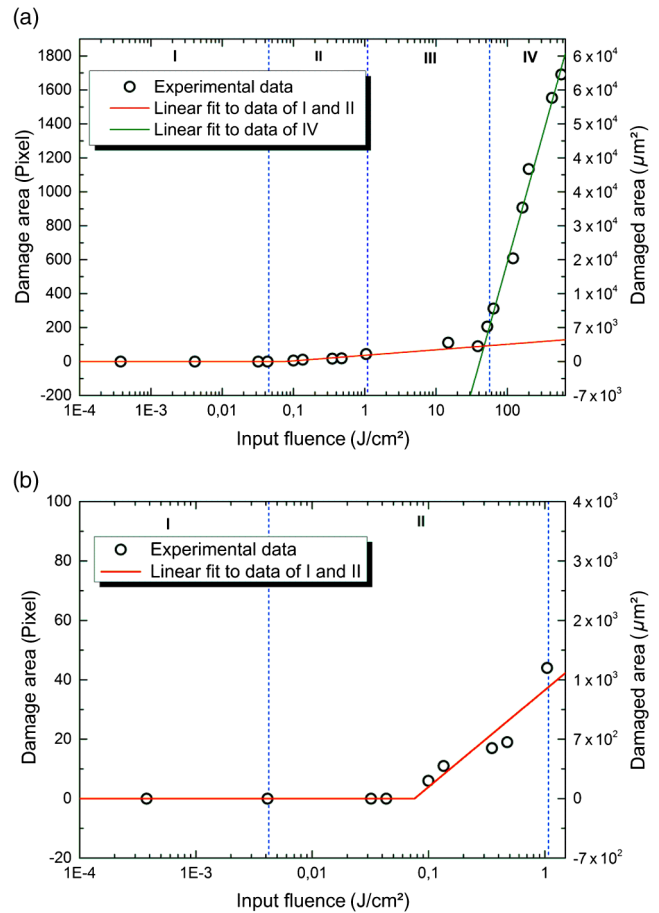
Fig. 6 Damaged area size of a monochrome CMOS camera as a function of pulsed laser fluence in semilog plot: (a) full data and (b) section of the full data consisting damage types I and II. The vertical blue dashed lines demarcate different stages of damage phenomenon.
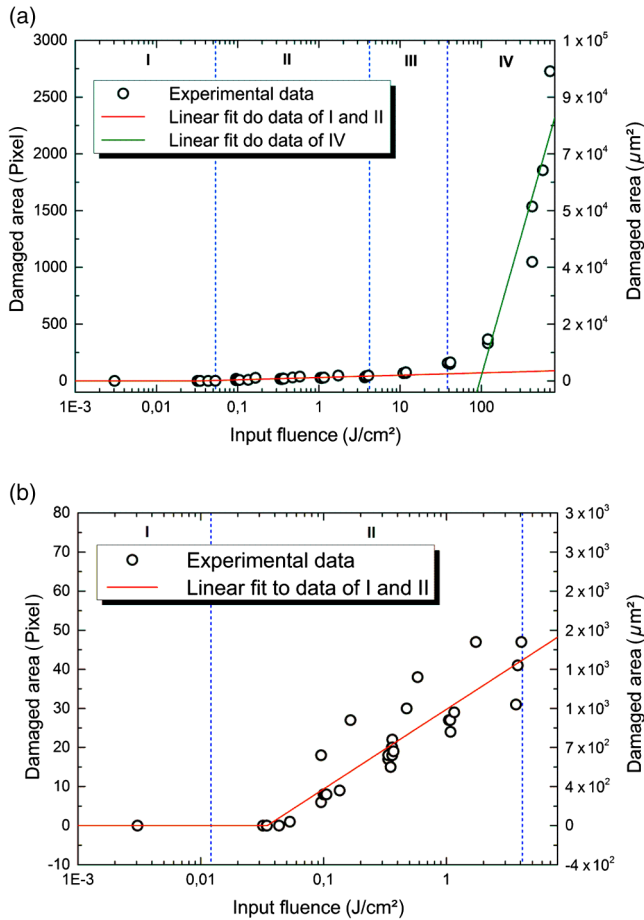
Fig. 7 Size of the damaged area of a color CMOS camera as a function of pulsed laser fluence in semilog plot: (a) full data and (b) section of the full data consisting damage types I and II. The vertical blue dashed lines demarcate different stages of damage phenomenon.

For pulsed laser radiation, we identified four different types of laser-induced impact on the cameras, which we classified in four groups (see Table 2). Each group was marked by vertical blue dashed lines in the graphs of Fig. 6–8. In the case of CW-radiation, only spot damage and in a few occasions line damage occurred.
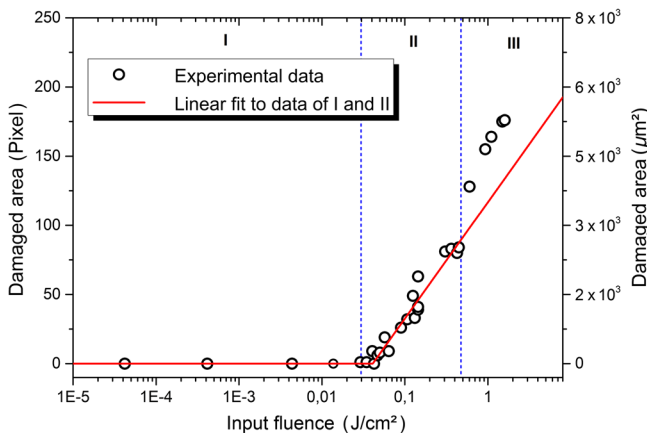
Fig. 8 Size of the damaged area of a color CCD camera as a function of pulsed laser fluence in a semilog plot. The blue dashed lines demarcate different stages of damage phenomenon.

3.3 Observation, Morphology, and Threshold of Pulsed Laser-Induced Damage on CMOS Cameras

In the case of the monochrome CMOS cameras exposed to pulsed laser light, first sensor damages were observed at a fluence of 0.1 J/cm^2. No damage was observed below a level of 0.043 J/cm^2. The damages appear as white "hot pixels" in the dark and in the bright images [see Fig. 3(1–3)]. This may indicate that pulsed laser radiation causes a change in the bandgap of the semiconductor or a change in the insulation area resulting in an increasing leakage current. Whether there is incident light or not, white pixels are quite apparent. The shape of the damage was mainly circular and slightly elongated in the horizontal direction. At further increased fluence, the spot damage started to develop star-shaped edges around a circular center, starting from a value of 14.9 J/cm^2. In Fig. 3([3b]), such peaks can also be recognized at fluence levels at which line damage occurs, but not to a great extent. Line damage, an emergence indicating that a whole line in the horizontal and/or in vertical direction became inoperative, started at a value of about 1.42 J/cm^2. In the vertical direction, the line damage extended steadily to the borders of the detector. At high fluence values, the line damage on the right-hand side of the damaged area was stronger than the line damage on the left-hand side. Line damage may be caused by signal interruption because of the device circuit fuses being cut. There was no visible difference in the shape of the damaged area for the bright images and the dark-frame. The graph in Fig. 6(a) shows the damaged area as a function of pulsed laser fluence for the monochrome CMOS camera. We performed two linear fits [cf. Eq. (4)] to the data with different slopes. For the fit concerning the data of groups I and II [see the red line in Fig. 6(b)], we estimated a damage threshold of $F_{th} = (0.076 \pm 0.019)$ J/cm^2 and a corresponding RBD of $2\omega_0 = (18.9 \pm 3.8)$ μm. This estimated value corresponds to the previously measured beam diameter, so we can assume that the physical damage of the sensor and the disturbance in the corresponding output image are comparable. As soon as the spot damage starts to develop as star shaped, the linear fit to the data becomes a different slope [see green line in Fig. 4(a)], which would result in another RBD of $2\omega_0 = (1285 \pm 5)$ μm. Consequently, we can conclude that the disturbance in the output image of the camera grows faster than the physical damage on the sensor chip. We interpreted the intersection of the green and the red line as the beginning of the formation of the star-shaped character at a fluence value of $F_s = 47.2$ J/cm^2.

The formation of damage by irradiating color CMOS cameras started to grow at a level of $F = 0.053$ J/cm^2. No damage was observed below 0.043 J/cm^2. Line damage was observed at a level of $F = 3.7$ J/cm^2. Star-shaping started at a value of 38.6 J/cm^2. The shape of the spot damage was also circular and slightly elongated in the horizontal direction. No difference in the composition of the damage in dark and the bright images was observed. It is striking that the damaged pixels appeared predominantly green, both in the dark image and in the bright image [see Fig. 3(4–5)]. Only in the case of higher pulse energies, did the damaged pixels appear mainly white in the center of the damaged area and green at the edges of the area in the dark image. It is remarkable that in the flat-field image, the edges of the

damaged area appeared in red [see Fig. 3(6)]. The line damage represented itself in red, yellow, and black lines or in blue and black lines for lower energies. Only in case of higher energy, was there a bunch of black lines with blue lines at one outer border and red as well as yellow lines at the other border. The camera sensor was completely destroyed in the sense that the output image no longer reacted to incident light, at a level of 2.9 kJ/cm². The red curve in Fig. 7 represents the dependence of the damaged area versus input fluence for low laser pulse energy. From the linear fit, we estimate a damage threshold of $F_{th} = (0.035 \pm 0.009)$ J/cm² and an RBD of $2\omega_0 = (14.9 \pm 4.5)$ μm. The intersection of the green and the red curve lies at a fluence value of $F_s = 102$ J/cm². The fact that the damage threshold of the color CMOS camera was lower than the damage threshold of the monochromatic device is an indication that the first damage in color cameras emerges in the Bayer filter.

3.4 Observation, Morphology, and Threshold of Pulsed Laser-Induced Damage on CCD Cameras

For monochrome CCD cameras, the formation of damage started at a fluence of $F = 0.032$ J/cm². No damage was observed below a level of 0.004 J/cm². Line damage was also observed and started at a fluence value of $F = 0.35$ J/cm². At a fluence value of $F = 147$ J/cm², the whole sensor was broken. The damage appeared as a white "hot pixel" in the dark image as well as in the bright image [Fig. 3(7–9)]. Line damage evolved only in the vertical direction. The damage on the camera started as point damage and, in contrast to CMOS cameras, the damage elongated in the vertical direction as the energy increased, starting at a fluence of $F = 0.14$ J/cm². This behavior was also observed in other works.[23] For most CCD cameras, the electrodes in each pixel are arranged in such a way that the charge is transferred in the vertical direction along the column to the final row (readout register). To avoid the charges escaping laterally, there are some "channel-stops" implanted near to the surface to isolate the charge packets from adjacent columns. In the case of strong irradiation, the created charge carriers prefer the vertical direction. The shape of the damage was equal in both the dark-frame and flat-field images. Due to the destruction of the sensor, we did not receive enough data to perform linear curve-fitting.

In the case of the color CCD camera, at first glance the bright image exhibited a different red level baseline after each shot. The formation of spot damage started at a level of $F = 0.034$ J/cm² and no damage was observed beneath a fluence value of 0.014 J/cm². Line damage occurred at a level of $F = 0.49$ J/cm² and appeared red, blue, or yellow. At a level of 3.16 J/cm², the camera was destroyed. The damage occurred almost circularly above a fluence of 0.064 J/cm² and appeared green in the dark image and yellow in the bright image. The damage exhibited the same shape in the bright and the dark images. Due to the red background in the image, the damaged pixels, which are related to the green channel of the sensor, appeared in yellow. The damage shape elongated in the vertical direction with increasing energy. At higher laser energy, the color of the damaged area turned mostly white, but at the outer border of the damage, all colors are represented. From the fit in Fig. 8, we got

a damage threshold $F_{th} = (0.041 \pm 0.003)$ J/cm² and an RBD of $2\omega_0 = (37 \pm 5)$ μm.

3.5 Observation, Morphology, and Threshold of CW-Laser-Induced Damage on CMOS Cameras

In contrast to pulsed laser-induced damage, no visible damage occurs in the dark image. Therefore, only the bright images were used to analyze the visible damage. First damage occurred in case of the monochrome CMOS cameras for exposure times of 0.25, 1, 5, and 10 s at a power density of 85, 85, 57, and 49 kW/cm², respectively. The shape of the damage was mostly circular and slightly blurred, because the damaged pixel became less sensitive but did not fail completely. The damage appeared dark in the flat-field image in opposition to the pulsed-laser damage, where the damage appeared white in the flat-field image. We also observed line damage starting from a power density of 196 kW/cm². From the fit in Fig. 9(a), we got a damage threshold depending on the exposure time of $F_{th} = [75 \pm 7, 73 \pm 13, 56 \pm 4, 48 \pm 3]$ kW/cm². Obviously, the slope of the lines in red and black are different from those in green and blue. According to Eq. (4), different slopes are associated with different RBD $2\omega_0 = [14 \pm 5, 16 \pm 4, 20 \pm 3, 21 \pm 3]$ μm.

In the case of the color CMOS cameras, damage started at a power density of 46 kW/cm² for an exposure time of
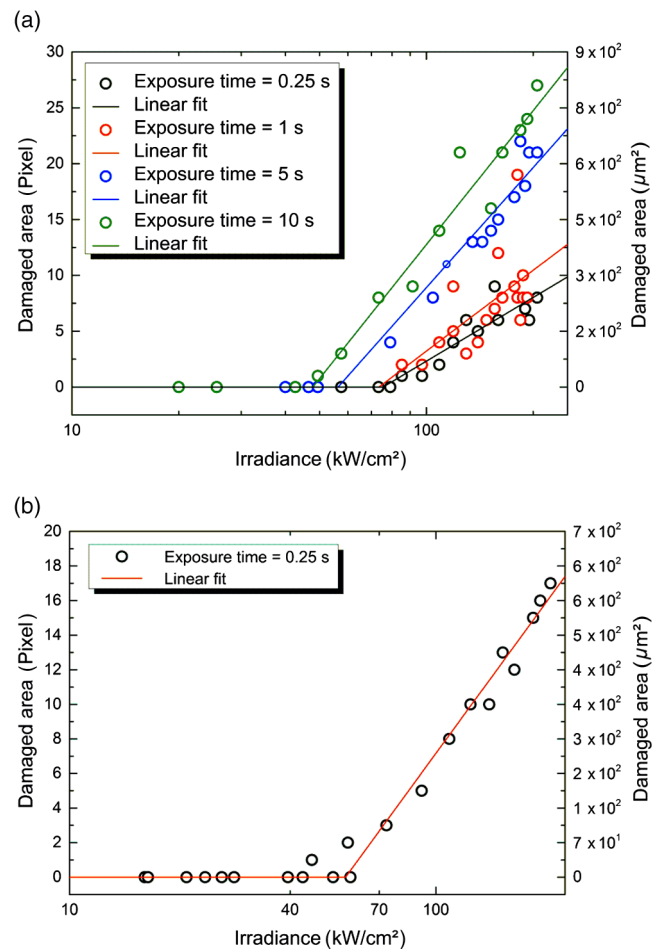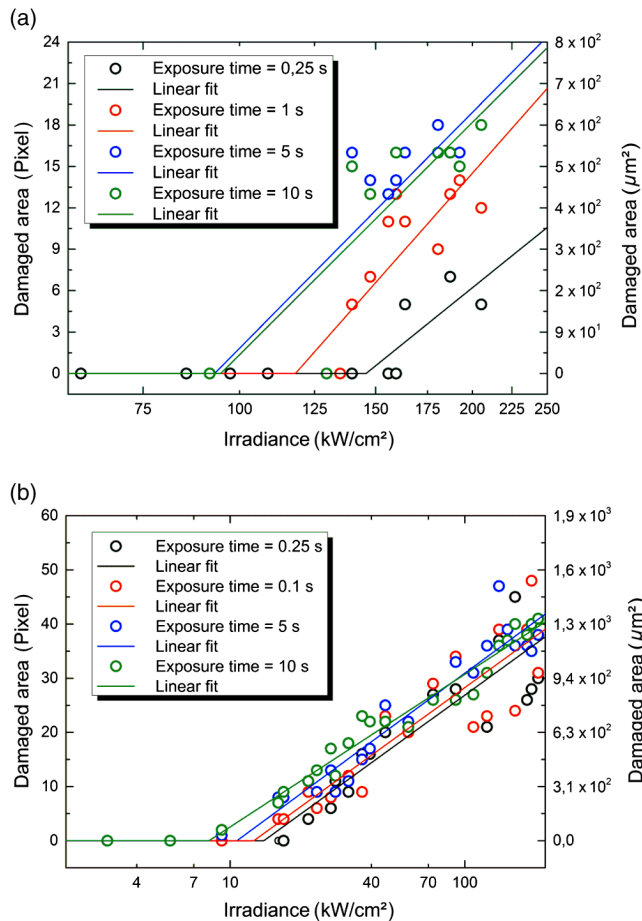

Fig. 9 Size of the damaged area of a CMOS camera versus power density of a CW-laser in a semilog plot: (a) monochrome camera and (b) color camera.

0.25 s. No line damage was observed. Damaged pixels seemed almost purple, in other words, a combination of blue and red pixel values. Just as it was in the case of damage to the monochromatic device, the shape appeared almost circular and blurred. From the fit in Fig. 9(b), we got a damage threshold of $F_{th} = (56.7 \pm 1.8)$ kW/cm^2 and an RBD $2\omega_0 = (12.6 \pm 0.5)$ μm.

3.6 Observation, Morphology, and Threshold of CW-Laser-Induced Damage on CCD Cameras

For the monochrome CCD camera, it was quite challenging to cause damage to the sensor. Damage started to occur for exposure times of 0.25, 1, 5, and 10 s at power densities of 163, 139, 139, and 139 kW/cm^2, respectively. No damage occurred below a value of 135 kW/cm^2 for exposure times of 1, 5, and 10 s and below a value of 159 kW/cm^2 for an exposure time of 0.25 s. The shape of damage is almost circular and the damaged pixels are dark in the output image. From the fit in Fig. 10(a), we got a damage threshold of $F_{th} = [146 \pm 9, 118 \pm 9, 93 \pm 19, 95 \pm 23]$ kW/cm^2 and an RBD $2\omega_0 = [22 \pm 3, 27 \pm 3, 25 \pm 3, 25 \pm 3]$ μm, respectively.

In case of the color CCD camera, we observed the same behavior as in case of the pulsed-laser-induced damage to the camera of the same type. The bright image exhibited a different red baseline after each shot. First damage for exposure times of 0.25, 1, 5, and 10 s started at a power density of 16, 16, 9, and 9 kW/cm^2 and no damage occurred below a level of 9.2, 9.2, 5.5, and 5.5 kW/cm^2. No line damage was observed. The damage shape was circular. Damaged pixels were almost purple or deep red because of the high red levels. The information of the green pixels was reduced, but they were not completely insensitive. From the fit in Fig. 10(b), we estimated a damage threshold of $F_{th} = [14 \pm 2, 13 \pm 2, 11 \pm 1, 8.1 \pm 0.8]$ kW/cm^2 and an RBD of $2\omega_0 = [18.5 \pm 3.6, 18.5 \pm 3.6, 18.6 \pm 3.6, 17.5 \pm 3.8]$ μm.

3.7 Observation, Morphology, and Threshold of CW-Laser-Induced Damage on Digital Micromirror Device

Initially, damage appeared as pixels with reduced intensity if the DMD was illuminated. Due to the fact that one micromirror was represented by 1.5 pixel in the camera image, there are always areas which are a combination of damaged mirrors and undamaged ones. Laser-induced damage to the micromirrors could cause a decrease in reflection or could destroy the tilt mechanism. Damage on the DMD started at a power density of 19.3 kW/cm^2 for an exposure

Fig. 11 Size of the damaged area of the DMD versus power density of a CW-laser source.
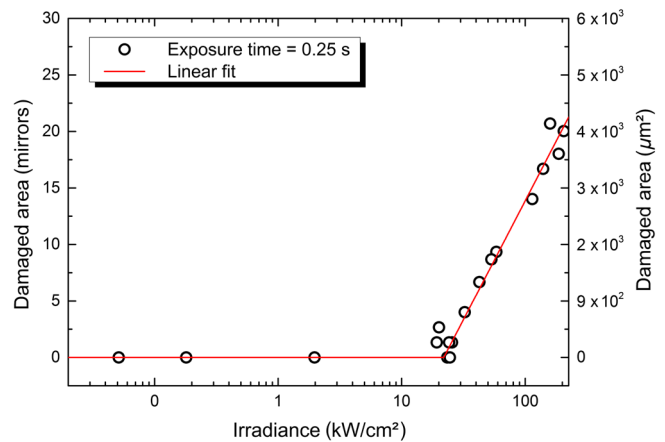

Fig. 10 Size of the damaged area of a CCD camera versus power density of a CW-laser in a semilog plot: (a) monochrome camera and (b) color camera.

Table 3 Results from the 1-on-1 test for pulsed laser sources.

Test sample	Damage threshold experimental data (J/cm^2)	Damage threshold fit to data (J/cm^2)	Line-damage threshold (J/cm^2)	Star-shape[a] or vertical elongated[b] threshold (J/cm^2)
CMOS				
Mono	0.099	0.08 ± 0.02	14.9	47.2
Color	0.053	0.035 ± 0.01	38.6	102
CCD				
Mono	0.032	—	0.35	0.14
Color	0.034	0.041 ± 0.003	0.49	—

[a]In case of damage to CMOS sensor.
[b]In case of damage to CCD sensor.

Table 4 Results from the 1-on-1 test for CW-laser sources.

Test sample	Damage threshold experimental data (kW/cm²)				Damage threshold fit (kW/cm²)			
Exposure time (s)	0.25	1	5	10	0.25	1	5	10
CMOS								
Mono	85	85	57	49	75 ± 7	73 ± 15	56 ± 4	48 ± 3
Color	46	—	—	—	56.7 ± 1.8	—	—	—
CCD								
Mono	163	139	139	139	146 ± 9	118 ± 9	93 ± 19	95 ± 21
Color	16	16	9	9	14 ± 2	13 ± 2	11 ± 1	8.1 ± 0.8
DMD	19.3	—	—	—	21.9 ± 1.2	—	—	—

time of 0.25 s. No damage was observed below a power density of 1.9 kW/cm². The damage on the DMD sensor is almost circular. The fit (red slope in Fig. 11) from Eq. (4) led to a damage threshold of $(21.9 \pm 1.2) \mathrm{kW/cm}^2$ and an RBD of $2\omega_0 = (15 \pm 4)\ \mu\mathrm{m}$.

4 Conclusion

We have studied the formation and evolution of laser-induced damage to CMOS and CCD cameras by means of pulsed and CW-laser radiation. The results for pulsed laser radiation are listed in Table 3. The damage was observed in both the bright images and the dark images. It is worth mentioning that starting from a defined value of laser fluence the damage on CMOS evolved as star shaped and on CCD damage elongated in the vertical direction. The color cameras exhibited the lowest damage threshold. Generally, the damage threshold of the CCD cameras was lower than that of the one of the CMOS cameras.

We also examined the formation and evolution of CW-laser-induced damage to CMOS and CCD cameras on the one hand and for the DMD (see Table 4) on the other hand. Damage only manifested itself in the bright image. Damage to the color devices occurred earlier than damage to the monochromatic cameras. The damage threshold of the DMD lies in the magnitude of the color CCD camera, but significantly below those of the other devices. For the latter sensors, a DMD could be installed as a sacrificial element in front of the sensor. Further investigations should contain pulsed laser-induced damage to the DMD with pulse lengths on the order of nanoseconds and picoseconds (also to the CMOS and DMD). Additionally, we will investigate the physical damage on the sensor, which is visible under the microscope.

References

1. G. Ritt, D. Walter, and B. Eberle, "Research on laser protection: an overview of 20 years of activities at Fraunhofer IOSB," *Proc. SPIE* **8896**, 88960G (2013).
2. B. Eberle et al., "Understanding how nanoparticle geometry may influence optical limiting," *SPIE Newsroom* (18 December 2012).
3. G. Ritt and B. Eberle, "Automatic laser glare suppression in electro-optical sensors," *Sensors* **15**(1), 792–802 (2015).
4. G. Ritt and B. Eberle, "Electro-optical sensor with spatial and spectral filtering capability," *Appl. Opt.* **50**(21), 3847–3853 (2011).
5. G. Ritt and B. Eberle, "Automatic suppression of intense monochromatic light in electro-optical sensors," *Sensors* **12**(10), 14113–14128 (2012).
6. G. Ritt et al., "Protection performance evaluation regarding imaging sensors hardened against laser dazzling," *Opt. Eng.* **54**(5), 053106 (2015).
7. M. F. Becker et al., "Laser-induced damage to silicon CCD imaging sensors," *Proc. SPIE* **1105**, 68–77 (1989).
8. M. F. Becker et al., "Laser-induced functional damage to silicon CCD sensor arrays," *Proc. SPIE* **1624**, 67–79 (1992).
9. F. Guo et al., "Damage effect on CMOS detector irradiated by single-pulse laser," *Proc. SPIE* **8905**, 890521 (2013).
10. Texas Instruments, "DLP® 0.7 XGA 2xLVDS type A DMD," in *DLPS026A Datasheet* (2012).
11. Texas Instruments, "Laser power handling for DMDs," *DLPA027 Datasheet* (2012).
12. A. R. Faustov, M. R. Webb, and D. R. Walt, "Note: toward multiple addressable optical trapping," *Rev. Sci. Instrum.* **81**(2), 026109 (2010).
13. X. Wang et al., "Laser-induced damage threshold of silicon in millisecond, nanosecond, and picosecond regimes," *J. Appl. Phys.* **108**, 033103 (2010).
14. D. Ristau, *Laser-Induced Damage in Optical Materials*, CRC Press/Taylor & Francis Group, New York (2015).
15. A. E. Siegman, *Lasers*, pp. 663–667, Oxford University Press, University Science Books, Oxford, England (1986).
16. J. A. Seibert, J. M. Boone, and K. K. Lindfors, "Flat-field correction technique for digital detectors," *Proc. SPIE* **3336**, 348 (1998).
17. M. J. Liu, "Simple technique for measurements of pulsed Gaussian-beam spot sizes," *Opt. Lett.* **7**(5), 196–198 (1982).
18. Y. Cai et al., "Experimental study of the damage of silicon photoelectric detector materials induced by repetitively pulsed femtosecond laser," *Proc. SPIE* **8796**, 87960I (2013).
19. G. M. Gusakov, A. A. Komarnitskii, and A. I. Frolov, "Simple method of determining the size of small-diameter Gaussian beams," *Meas. Tech.* **30**, 762–764 (1987).
20. J. Jandeleit et al., "Picosecond laser ablation of thin copper films," *Appl. Phys. A* **63**(2), 117–121 (1996).
21. R. M. Wood, "Laser induced damage thresholds and laser safety levels. Do the units of measurement matter?" *Opt. Laser Technol.* **29**(8), 517–522 (1998).
22. N. V. Lednev et al., "Single-shot and single-spot measurement of laser ablation threshold for carbon nanotubes," *J. Phys. D: Appl. Phys.* **46**(5), 052002 (2013).
23. N. Machet et al., "Study of the mechanism of electronic diffusion in a CCD camera subject to intense laser illumination," *RADECS* **97**, 417–423 (1997).

Bastian Schwarz has been a research scientist at Fraunhofer IOSB, Ettlingen, Germany, since 2013. He graduated in physics from the University of Freiburg in 2012 and worked at the Kiepenheuer Institute for Solar Physics. Since 2013, his research areas include laser protection and laser damage performance.

Gunnar Ritt is a research associate at Fraunhofer IOSB, Ettlingen, Germany. He received his diploma and PhD degrees in physics from the University of Tübingen, Germany, in 1999 and 2007, respectively. His main research focus is on laser protection.

Michael Koerber has been a research scientist at Fraunhofer IOSB, Ettlingen, Germany, since 2013. He is part of the optical countermeasure and laser protection group and participated in several projects. He received his master of science degree in physics from the University of Konstanz in 2012. He works in the field of laser spectroscopy, nonlinear optics, femtosecond optics, and optical countermeasures.

Bernd Eberle is a senior scientist at Fraunhofer IOSB in Ettlingen, Germany, where he is head of the optical countermeasure and laser protection group. He received his diploma degree in physics at the University of Konstanz in 1983. He received his PhD degree in physics at the University of Konstanz in 1987. His research activities comprise laser technology, laser spectroscopy, nonlinear optics, femtosecond optics, optical countermeasures including protection against laser radiation and imaging laser sensors.